

Optical remote sensing of benthic habitats and bathymetry in coastal environments at Lee Stocking Island, Bahamas: A comparative spectral classification approach

Eric M. Louchard, R. Pamela Reid, and F. Carol Stephens

University of Miami, Rosenstiel School of Marine and Atmospheric Science, 4600 Rickenbacker Causeway, Miami, Florida 33149

Curtiss O. Davis, Robert A. Leathers, and T. Valerie Downes

Code 7212, Naval Research Laboratory, 4555 Overlook Avenue SW, Washington, D.C. 20375

Abstract

Remote sensing is a valuable tool for rapid identification of benthic features in coastal environments. Past applications have been limited, however, by multispectral models that are typically difficult to apply when bottom types are heterogeneous and complex. We attempt to overcome these limitations by using a spectral library of remote sensing reflectance (R_{rs}), generated through radiative transfer computations, to classify image pixels according to bottom type and water depth. R_{rs} spectra were calculated for water depths ranging from 0.5 to 20 m at 0.5- to 1.0-m depth intervals using measured reflectance spectra from sediment, seagrass, and pavement bottom types and inherent optical properties of the water. To verify the library, computed upwelling radiance and downwelling irradiance spectra were compared to field measurements obtained with a hyperspectral tethered spectral radiometer buoy (TSRB). Comparisons between simulated spectra and TSRB data showed close matches in signal shape and magnitude. The library classification method was tested on hyperspectral data collected using a portable hyperspectral imager for low light spectroscopy (PHILLS) airborne sensor near Lee Stocking Island, Bahamas. Two hyperspectral images were classified using a minimum-distance method. Comparisons with ground truth data indicate that library classification can be successful at identifying bottom type and water depth information from hyperspectral imagery. With the addition of diverse sediments types and different species of corals, seagrass, and algae, spectral libraries will have the potential to serve as valuable tools for identifying characteristic wavelengths that can be incorporated into bottom classification and bathymetry algorithms.

Remote sensing has long been used to analyze terrestrial features, such as soil mineral content, foliage density and type, and surface elevation (Curran et al. 1992; Palacios-Orueta and Ustin 1998; Rollin and Milton 1998; Kokaly and Clark 1999). Satellite and airborne sensors are well suited to terrestrial observations in the visible and infrared range. These sensors are more limited, however, when used over oceans or lakes because of the low reflectance values of deep water (giving relatively poor signal-to-noise ratios) and the complexity of combined water and bottom signals in shallow water (Jerlov 1976). Most applications of marine remote sensing to date have been estimations of phytoplankton biomass and sea surface temperatures (SSTs). In these applications, it is generally assumed that all light from the ocean is either spectrally reflected from the upper several meters of the water column or thermally emitted from the first few millimeters at the surface. For biomass and SST applications in shallow water, visible radiation reflected from the bottom

is typically considered to be noise (Hu et al. 1998). Bottom radiation usually overwhelms the phytoplankton signal in shallow water, making measurements of water column properties unreliable in nearshore areas.

With the introduction of high-resolution multispectral and hyperspectral sensors, light reflected from the bottom in shallow water can be spectrally analyzed, and bottom types can be discriminated by their reflectance signatures. Multispectral data analyses with one-dimensional radiative transfer models has proven to be effective in estimating coral densities, deriving water optical properties, and mapping bathymetry (Lyzena 1981; Philpot 1988; Lee et al. 1997; Holden and LeDrew 1998). These analyses can be further enhanced by the introduction of hyperspectral data sets, which can be analyzed using traditional spectroscopic techniques, such as spline smoothing, gaussian peak fitting, and derivative analysis.

A practical application of hyperspectral data analysis is presented in this paper. We illustrate a comparative technique that is used to characterize benthic habitats and to estimate bathymetry from remotely sensed images of a shallow-water carbonate environment in the vicinity of Lee Stocking Island, Bahamas. Remote sensing reflectances (R_{rs}) of individual pixels in hyperspectral images are compared to simulated R_{rs} spectra, created using measured values of bottom reflectance and water inherent optical properties (IOP's), at water depths ranging from 1 to 20 m. This technique provides information about the transmission to the surface of spectral signals from various bottom types and indicates which spec-

Acknowledgments

This work was supported by the Office of Naval Research, Environmental Optics Program Awards N000149710010 and N00149910130. We thank Robert Maffione, Richard Zimmerman, and Ken Voss for discussion on optical theory; Charles Mazel for the loan of a DiveSpec instrument; Emmanuel Boss and Ronald Zaneveld for IOP measurements; Jeffrey Bowles, Mary Kappus, Megan Carney, and Bosch Aerospace for PHILLS data collection; and other members of the CoBOP program and the staff of the Caribbean Marine Research Center at Lee Stocking Island, Bahamas, for additional field assistance.

tral regions could be used in future analytical models of benthic characterization. By combining spectral information reported in this paper with results from other research in the ONR program on Coastal Benthic Optical Properties (CoBOP), remote sensing models can be created that effectively map the bottom in environments beyond the carbonate Bahama platform of Lee Stocking Island.

One-dimensional radiative transfer models—The creation of bottom maps using standard shipboard instrumentation and sampling techniques is a time-consuming process. Consequently, remote sensing models have been developed that calculate bathymetry or bottom reflectance using a one-dimensional radiative transfer equation, assuming that water inherent optical properties are uniform and the bottom is a flat Lambertian reflector (Lyzena 1981; Philpot 1988; Maritorena et al. 1994). Algorithms in these models describe the exponential attenuation of radiance at individual wavelengths through the water column and predict the radiance received at a remote detector by factors such as atmospheric effects, transmission across the air–sea interface, illumination intensity, and incident angle. These algorithms provide a means for creating bathymetric maps from remotely sensed multispectral data, such as from Landsat 7, if bottom type maps and in situ reflectance measurements for bottom types are available (Philpot 1988, 1990). By inverting the algorithm, bottom reflectance can be mapped if bathymetric soundings are available. This approach for bottom classification is cumbersome, however, when calculating reflectance for the full spectrum of wavelengths available in hyperspectral data

Another problem with using one-dimensional models for bathymetric mapping is that the algorithms were not designed to distinguish between complex bottom spectra. As a result, bottom types are typically oversimplified. The assumption is commonly made, for example, that sediments in a region are laterally homogeneous and share a single reflectance spectrum (e.g., Harris and Kowalik 1994). Such an assumption is, however, unrealistic and ignores spectral differences associated with heterogeneity in sediment composition, grain shape, grain size, and epifaunal assemblages (Hiroi and Pieters 1992, 1994; Clark et al. 1993; Brotas et al. 1995; Patterson et al. 1998; Karnieli et al. 1999).

The variability in reflectance exhibited by complex, heterogeneous bottom types complicates simple bathymetric models, such as that used by Harris and Kowalik (1994). Bottom diversity must be accurately mapped in order to estimate bathymetry from remote sensing images. Multispectral data typically do not contain enough spectral information to differentiate between complex bottom types. In contrast, hyperspectral data, characterized by a high number of spectral bands, are capable of capturing this diversity. The detailed spectral information available in hyperspectral images provides an opportunity to develop new approaches for analyzing and modeling benthic reflectance.

Spectral library approach—The use of spectral libraries to classify remote sensing images presents an alternative approach to using one-dimensional radiative transfer models. In the library approach, remote sensing reflectance (R_{rs}) of

individual pixels in the images are compared to simulated R_{rs} spectra created using measured values of bottom reflectance and water inherent optical properties. This approach enables identification of diverse bottom types with complex compositional variations.

An additional benefit of using a library approach to classify hyperspectral remote sensing data is that the library data can be analyzed using the tools of laboratory spectroscopy, such as derivative analysis. This enables identification of diagnostic spectral regions and shapes (Huguenin and Jones 1986), which can be incorporated into future models for estimating bathymetry or classifying bottom types. Derivative spectroscopy has proven especially useful in enhancing minute fluctuations in reflectance spectra and separating absorption features of closely related pigments (Butler and Hopkins 1970). Analytical chemists working in remote sensing have used derivative spectroscopy for many years to eliminate background signal and to resolve overlapping features. A primary application has been to remove soil background interference from leaf absorption spectra, facilitating the identification of pigment and chemical composition, as well as tracking physiological changes in plant canopies (Demetriades-Shah et al. 1990; Curran et al. 1992; Rollin and Milton 1998; Kokaly and Clark 1999). Derivative analysis was also applied to marine optical data to identify and quantify seagrass from mixed spectra at Lee Stocking Island, Bahamas (Zimmerman and Wittlinger 2000).

Derivative analysis and other spectroscopic techniques will become more valuable in the future as the amount of data from hyperspectral systems expands. Large data sets can be processed quickly into smaller portions of useful information, enabling hyperspectral imaging to be used for real-time coastal observation, object detection (search and rescue, recovery, salvage, threat assessment, etc.) and bathymetry retrieval.

Research objectives and study site—The goal of the present research was to use a comparative method of spectral library matching to classify bottom types and estimate bathymetry in remotely sensed images of shallow coastal areas. The technique is similar to that used by the USGS for mineral or vegetation mapping with multispectral sensors (Clark et al. 1992, 1995) but uses the increased information content available in hyperspectral imaging.

Research was conducted at Lee Stocking Island (LSI), Bahamas, located near the southern end of Exuma Cays (Fig. 1), as part of the CoBOP project sponsored by the U.S. Office of Naval Research. The excellent water clarity of the shallow-water Bahama platform makes this an ideal spot for conducting remote sensing research. Major benthic features are apparent from the air, including seagrass beds, shallow shoals, and pavement channels. The research involved five major steps: (1) data collection, (2) analysis of bottom reflectance, (3) creation and verification of a spectral library, (4) image classification and error assessment, and (5) spectroscopic analysis of library spectra.

Data collection

Data for the project were collected during four field sessions, each 3 weeks in duration, at the Caribbean Marine

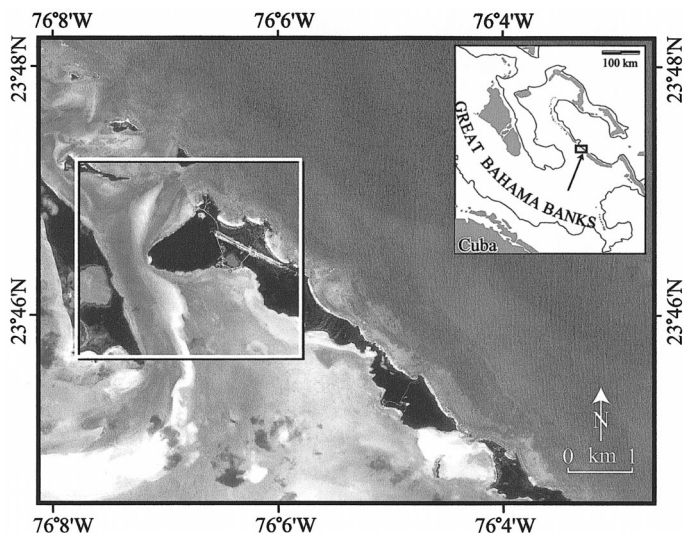


Fig. 1. Area surrounding Lee Stocking Island, Exumas, Bahamas, as seen from the IKONOS satellite sensor in multispectral mode (blue) at 4 m resolution. Box indicates the area shown in Fig. 2.

Research Center, Lee Stocking Island, in May/June 1998–2001. A variety of information types were required for the development and ground truthing of the spectral library used in benthic classification. Data collection included acquisition of airborne hyperspectral data, field analysis of bottom types, and measurement of spectral reflectance, water inherent optical properties, upwelling radiance and downwelling irradiance (TSRB), and bathymetry, as follows.

Hyperspectral data—Hyperspectral images at LSI were collected as part of the CoBOP program using PHILLS (portable hyperspectral imager for low light spectroscopy), a system with high spectral and spatial resolution designed specifically for remote sensing of shallow coastal water (Davis et al. 2002). A preflight spectral calibration of the PHILLS was performed in the laboratory by imaging several different gas lamps (oxygen, mercury, argon, helium). The exact locations of known gas emission lines were obtained using the *atom.exe* program obtained from the National Institute of Standards and Technology (NIST). By pairing up measured emission lines with known lines, a relationship was derived between channel number and wavelength of the center of the channel.

Radiometric calibration of the PHILLS was performed using a 102-cm Spectralon-coated integrating sphere containing 10 halogen lamps (Labsphere). The intensity of the sphere at each lamp level was determined by performing a transfer calibration from a NIST-calibrated FEL lamp. Because the sphere source is red rich, a blue balancing filter was placed in front of the PHILLS lens to help level out the source spectrum. Calibration measurements were taken for 1, 2, 3, 4, 6, 8, and 10 lamps illuminated, and this was used to acquire a quadratic relationship between data counts and radiance for each pixel on the charge-coupled device (CCD).

During the deployment at Lee Stocking Island, the PHILLS system was carried on an Antonov biplane, trav-

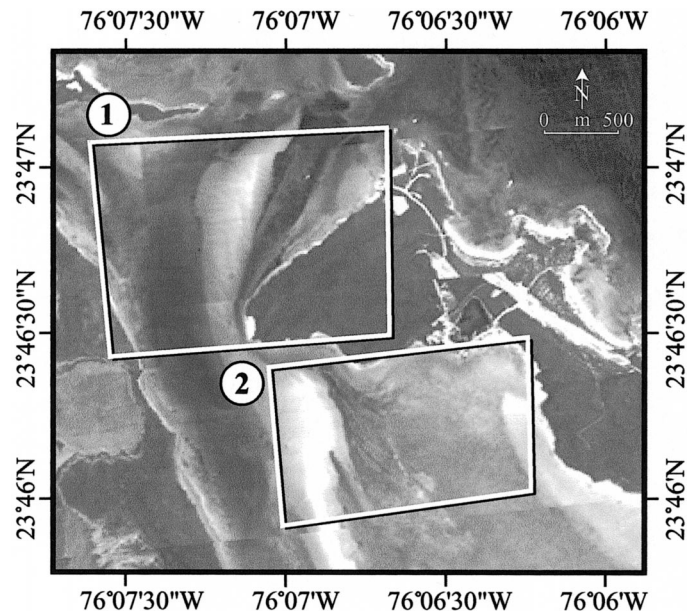


Fig. 2. Mosaic of flight lines imaged with a hyperspectral PHILLS camera at 1.25- × 1.25-m pixel resolution. White boxes indicate the study sites: Site 1, Adderly Cut; Site 2, Channel Marker buoy.

eling at a cruising speed of 45 m s⁻¹ and at an altitude of 2,360 m. The PHILLS camera produced images with a 1.25- × 1.25-m ground sample distance (GSD) and 1.25-km swath. Hyperspectral data were collected in 70 spectral channels of 4.65 nm, ranging from 400–725 nm. (Data were collected at additional channels above 725 nm, but these channels exhibited poor signal-to-noise ratios.)

PHILLS data used for the present study were acquired between 0930 and 1030 h (EST) on 1 June 1999 when the sun zenith angle was close to 30°. Ship reports indicated low wind (2 m s⁻¹), minimal ocean swell, and clear skies. Two sites were selected from flight lines for detailed analysis: Site 1 covered an area of approximately 1.85 km² in the vicinity of Adderly Cut; Site 2, in the vicinity of the Channel Marker buoy, covered an area of approximately 1.2 km² (Fig. 2).

Hyperspectral data from Sites 1 and 2 were atmospherically corrected by an improved version of the ATREM algorithm called TAFKAA with lookup tables generated by vector radiative transfer code to give water-leaving reflectance (L_w) (Gao et al. 2000). The tables used by TAFKAA were calculated with a full vector code that takes sea surface reflections into account and also deals with path-scattered radiance due to Rayleigh scattering and aerosols. Solar zenith and azimuth angles were calculated in the algorithm from the flight date, latitude, and longitude and were used to predict incident solar irradiance above the atmosphere. Absorption in the atmosphere was modeled using values of carbon dioxide (CO₂), nitrous oxide (N₂O), carbon monoxide (CO), methane (CH₄), and oxygen (O₂) estimated from typical tropical areas (Davis et al. 1999). The values of water vapor (H₂O) and ozone (O₃) were explicitly set to 1.1 atm-cm and 0.300 atm-cm respectively. The locations of prom-

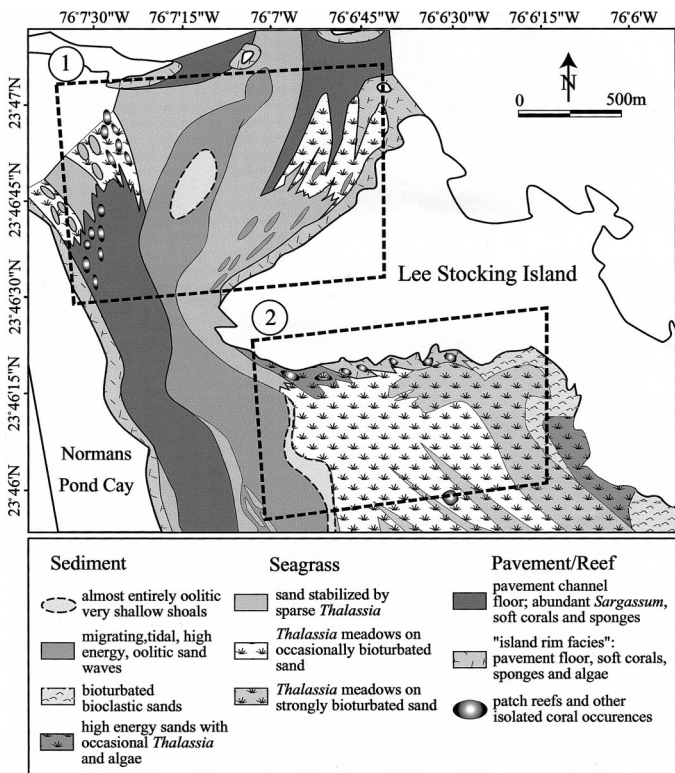


Fig. 3. Map of bottom types in the vicinity of Lee Stocking Island generated by diver observations; after Gonzalez and Eberli (1997). Boxes indicate study sites for the present paper: Site 1 Adlerly Cut; Site 2, Channel Marker buoy.

inent atmospheric absorption lines were used to fine tune the spectral calibrations.

In 1999, the calibrated PHILLS data had unrealistically low radiance values below 450 nm, resulting in negative values for atmospherically corrected R_{rs} . This is now known to be a calibration error caused by contamination of the radiometric data by light reflected in the camera from the zero-order portion of the diffraction pattern. In this study, the problem was resolved by adding a correction factor to every pixel in the image, calculated by subtracting the R_{rs} spectra of an offshore deep-water pixel from the R_{rs} spectra modeled in Hydrolight with an infinitely deep bottom.

In 1999, the PHILLS camera was not yet equipped with a GPS system that could perform per-pixel georeferencing. Therefore, the images were georeferenced based on ground

control points taken from an IKONOS multispectral image of LSI. The nonuniform motion of the aircraft caused by unsteady winds made georeferencing difficult. The georeferenced image of Site 1 matched well with the IKONOS image, but Site 2 contained a portion in the northwest corner that was warped beyond repair.

Field analyses of bottom types—In a previous study, a map of carbonate sedimentary facies in the vicinity of LSI (Fig. 3) was made by direct diver observations (Gonzalez and Eberli 1997). This map was used in the present study as a basis for sampling representative bottom types by snorkeling and SCUBA diving. In addition, underwater video recordings were filmed along transects with a 100-m spacing using a Sony DCR-TRV900 digital video camera housed in an Aqua Video case and mounted on a pole attached to the gunnel of a small boat.

Three primary bottom types were recognized in the two study sites: sediment, seagrass, and pavement/reef. Four types of carbonate sediment were differentiated based on depositional environment and grain composition (Table 1); each sediment type is characterized by distinct microalgal pigments and grain size (see Stephens et al. 2003 for methodology of sediment analysis). Field sampling indicated that ooid shoals (Fig. 3) are composed of two sediment types: ooid sand (Sediment Type 1, Table 1) and oolitic-skeletal sand (Sediment Type 2, Table 1). Ooids are nonskeletal grains with laminated coatings that form in high-energy tidal channels (Milliman 1974). Average chlorophyll a (Chl a) of the ooids is $1.6 \mu\text{g cm}^{-3}$; mean grain size is $275 \mu\text{m}$. Chl a content of the oolitic-skeletal sands ($0.8 \mu\text{g cm}^{-3}$) is lower than the pure oolitic sands, and average grain size is slightly larger ($430 \mu\text{m}$). The bioclastic sands of Fig. 3 are peloidal-skeletal sands (Sediment Type 3, Table 1) with a mean grain size of $600 \mu\text{m}$; although characteristically bioturbated, algal films developed on sediment surfaces between mounds give this sediment a high Chl a content ($6.36 \mu\text{g cm}^{-3}$). Sediment interspersed with seagrass (Fig. 3) is a mixture of ooids, peloids, and skeletal grains (Sediment Type 4, Table 1). Algal films are also commonly developed on these sands, giving average Chl a content of $3.78 \mu\text{g cm}^{-3}$; mean grain size is $262 \mu\text{m}$. Sediments from the small patch designated as “high-energy sands with occasional *Thalassia*” in Site 2 (Fig. 3) were not analyzed.

The dominant seagrass in the study areas is *Thalassia testudinum*. Seagrass density ranged from a sparse distribution of plants in sand to dense grass thickets. Bioturbation of

Table 1. Distinct sediment types found at Lee Stocking Island, Bahamas.

Sediment type	Environment	Grain composition	Chl _a ($\mu\text{g cm}^{-3}$)	Mean grain size (μm)
1	Migrating high-energy shoal	Oolitic sand	1.60	275
2	As above	Oolitic-skeletal sand	0.80	430
3	Quiet lagoon	Peloidal-skeletal sand with algal film	6.36	600
4	Stabilized sand in seagrass meadow	Oolitic-peloidal-foraminiferous sand in seagrass	3.78	262

sediments in the seagrass beds ranges from “occasionally bioturbated” to “strongly bioturbated” (Fig. 3).

The pavement and reefal areas are colonized by variable proportions of gorgonians (mainly light and dark varieties of *Psuedoplexaura*-like sp.), sponges, hydrocorals (mainly *Millepora alcicornis*), brown algae (mainly *Sargassum* sp.), and green algae (mainly *Microdictyon marinum*). Stony corals (primarily *Montastraea annularis*) form small isolated patch reefs.

Spectral reflectance—Reflectance measurements were made for representative sediment, seagrass, and pavement bottom types as follows.

Sediment: The primary methodology used to measure spectral reflectance of bottom sediments was a newly developed core technique. Ten sediment cores (22 mm diameter, 100 mm long) were taken with random spacing at each sampling site in a 0.25-m² area delineated with a square of plastic piping. Reflectance was measured by placing the core tube in a custom-designed holder constructed from a solid plastic cylinder, which was cut into a hollow shell. A hole in the top of the cylinder allowed an Ocean Optics RP200-7 Reflection Probe to be held at 0° to the sediment surface. An Ocean Optics S2000 UV-VIS spectrometer (grid #2, 50- μ m slit) was connected to the RP200-7 by a 200- μ m fiber-optic cable and was cojoined to an Ocean Optics LS-1 tungsten halogen light source, which was warmed up for 20 min to stabilize the lamp output spectra. Reflectance was measured from 190 to 890 nm in 2,048 channels (approximately 0.30 nm dispersion). Sediments in the cores were kept submerged in seawater during measurement; leaked water was replaced with filtered seawater up to the level of the optical probe sensors. Interfering organisms, such as copepods swimming up to the light fiber, were removed with a plastic pipette before measurement.

Light reflected from a sediment core was measured as spectrometer counts (CS_L) by the S2000. CS_L was measured three times for each sediment core, rotating the core 120° between measurements. Dark current (CS_D) was measured once for each set of 10 cores by taking three measurements of one core with the lamp off. This procedure reduced stress resulting from cycling the lamp on and off. Reflected light was also measured for an Ocean Optics WS-1 99% Spectralon reference standard, held in a PVC cylinder similar to that used for the sediment cores, with the RP200-7 probe clamped at a constant distance 25 mm normal to the WS-1 surface. The cylinder was filled with filtered seawater and microbubbles on the target surface removed with seawater squirted from a plastic pipette. Measurements of spectrometer counts under illumination (CR_L) and in darkness (CR_D) were made 10 times each. Radiance reflectance was calculated using an Ocean Optics WS-1 99% Spectralon reference standard as follows.

$$R = \left(\frac{CS_L - CS_D}{CR_L - CR_D} \right) \left(\frac{\text{int}_R}{\text{int}_S} \right) \quad (1)$$

CS_L and CS_D are the mean spectrometer counts measured for the sample in light and dark, respectively; int_S and int_R

Table 2. Average water IOPs measured at Site 2 on 1 Jun 99. Absorption coefficient (a) and beam attenuation coefficient (c) at nine wavelengths were measured with an *ac9*.

λ (nm)	a (m ⁻¹)	c (m ⁻¹)
412	9.45×10^{-2}	3.14×10^{-1}
440	7.43×10^{-2}	2.66×10^{-1}
488	4.06×10^{-2}	2.16×10^{-1}
510	2.90×10^{-2}	2.01×10^{-1}
532	2.26×10^{-2}	1.88×10^{-1}
555	1.57×10^{-2}	1.76×10^{-1}
650	4.33×10^{-3}	1.42×10^{-1}
676	5.70×10^{-3}	1.36×10^{-1}
715	0.0	1.27×10^{-1}

are the sample and standard integration times, and CR_L and CR_D are the mean spectrometer counts measured for the WS-1 reference standard in light and dark, respectively.

Seagrass: Seagrass beds were assumed to be uniform Lambertian bottoms with no canopy structure for the purpose of radiative transfer calculations. Reflectance for seagrass beds was therefore a linear mixture of measurements from the two major components: seagrass leaves and Sediment Type 4 (Table 1). The core holder used for sediments was used for reflectance measurements of *Thalassia testudinum*, the primary seagrass species in the study area. Reflectance measurements were made on a clean piece of leaf placed over a black bottom in a seawater-filled core tube. The leaf was cut to cover the entire bottom of the core tube.

Pavement/Reef: In situ reflectance measurements were made on pavement and the associated hard-bottom communities using a “Divespec” underwater spectrometer. The Divespec consists of a self-contained Ocean Optics S2000 spectrometer, with a 50-W halogen lamp and 200- μ m fiber-optic detector (Mazel 1997). Ten reflectance measurements were taken for each target, with wavelengths ranging from 400 to 750 nm (0.30 nm dispersion), using 99% Spectralon as reference. Reflectance was measured for bare pavement, gorgonians, hydrocorals, sponges, algae, and stoney coral.

Inherent optical properties of the water column—Inherent optical properties of the water (i.e., absorption coefficient, scattering coefficient, and scattering phase function) were measured in the vicinity of Lee Stocking Island as part of the CoBOP project, using a WET Labs *ac9* following the methods of Twardowski et al. 1999. On 1 June 1999, IOPs were measured at Site 2 on an outgoing tide, shortly after the PHILLS overflight (Table 2). Measurements of water IOPs at different points in the vicinity of LSI showed little spatial variation; therefore, the IOPs were assumed to be uniform over the study sites at the time of the PHILLS data collection.

TSRB measurements—A hyperspectral tethered spectral radiometer buoy (Satlantic) was used to measure upwelling radiance (L_u) and downwelling plane irradiance (E_d). The TSRB L_u and E_d sensors detected wavelengths ranging from 400 to 700 nm with 5-nm band spacing. L_u was measured

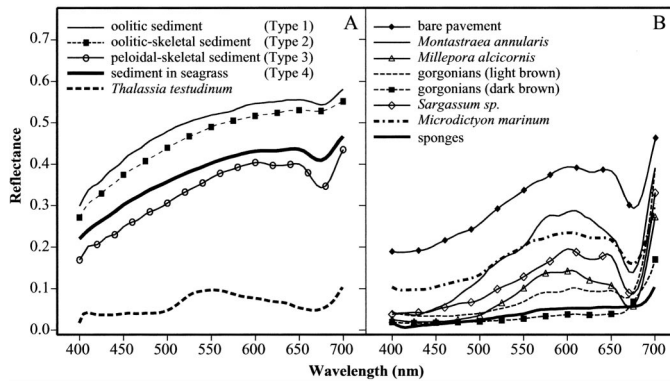


Fig. 4. Reflectance spectra used in building the spectral library. (A) Sediments and seagrass. (B) Pavement community.

0.66 m below the ocean surface with a 10° half-angle radiance sensor. E_d was measured at the top of the instrument, approximately 0.28 m above the ocean surface with a 180° cosine collector. To permit measurements in shallow water and to stabilize the TSRB, a custom-machined stainless steel sleeve weight was bolted around the bottom spar. The sleeve weight replaced the standard 20-m drogue weight. The TSRB was deployed over the side of a small 6-m boat and allowed to drift 5–20 m away until the shadow of the boat did not interfere with the instrument field of view. Position was measured using GPS. Measurements were recorded over Sediment Type 1 on 24 May 1999 and Sediment Type 3 on 1 June 1999.

Bathymetry—Depth maps were generated in the field using a Suzuki ES2025 echo sounder with a 50-kHz transducer. All measurements were tracked using GPS with Wide Area Augmentation System (WAAS) capability. The data were normalized to the average tidal depth of the PHILLS flight time (+0.4 m) using standard tide tables interpolated to the time interval of the sounder pings (0.7 s).

Analysis of bottom reflectance

Sediment—Reflectance spectra used to construct the spectral library showed distinct differences between sediment types (Fig. 4A). Reflectance was highest in sediment with minimal microalgal components such as oolitic-skeletal sand (Sediment Types 1 and 2) and lowest in sand with film (Sediment Types 3 and 4; see also Stephens et al. 2003). Major absorption features were evident in the reflectance spectra, including dips at 678 nm for Chl *a* and 498 nm for the carotenoids β -carotene, zeaxanthin, and diadinoxanthin (Kirk 1994). However, a majority of reflectance past 600 nm was lost when propagated through the water column. As a result, spectral differences between 400 and 600 nm were most important in analysis.

Differences in sediment grain size had a smaller effect on spectral reflectance than pigment composition but still caused a significant spectral divergence among Sediment Types 1 and 2. Sediment Type 2, composed of medium-coarse grains ($430 \mu\text{m}$), had a lower reflectance across the whole spectrum than fine-grained Sediment Type 1 (275

μm), even though it contained less Chl *a* (0.80 g cm^{-3} compared to 1.60 g cm^{-3}).

Grain composition is also a determinant of sediment reflection. Oolitic Sediment Types 1 and 2 were the brightest sands because of the highly reflective laminated carbonate coatings on these grains. Peloidal-skeletal sand (Sediment Type 3) was less reflective than the oolitic sand and was typically found in calm environments characterized by high concentrations of polymer biofilm.

Seagrass—The *Thalassia* leaf displayed a distinctive drop in reflectance from 550 to 680 nm because of Chl *a* absorption (Fig. 4A) and was lower at 700 nm than any other measured bottom type. Overall reflectance of the seagrass beds depended on the percentage of canopy cover compared to sediment.

Pavement/Reef—All of the measured parts of the pavement community showed distinctive spectral features (Fig. 4B), such as a prominent dip at 675 nm, a smaller dip at around 620 nm, and a steep rise after 700 nm. The rise after 700 nm and the lack of a steep single slope from 550 to 680 nm distinguished the pavement community from seagrass. Bare pavement appeared similar in spectral magnitude to Sediment Type 3, but displayed a steeper dip at 675 nm. *Sargassum* and *Microdictyon* were similar to gorgonians but had higher spectral magnitude. *Montastraea annularis* was differentiated from other pavement community members by its low reflectance in the blue from 400 to 450 nm and the steep rise in reflectance from 450 to 600 nm. Reflectance of sponges was almost identical to that of dark brown gorgonians.

Spectral library

Creation of the spectral library—A library of computer-simulated remote sensing reflectance (R_{rs}) and upwelling radiance (L_u) was created using the program Hydrolight (Sequoia). Remote sensing reflectance spectra were calculated at 0.5-m intervals to a depth of 10 m and at 1-m intervals from 10 to 20 m. In addition to simulated spectra of water leaving radiance, L_u was calculated at a depth of 0.66 m in order to compare simulations with TSRB measurements. Inputs to Hydrolight included the following.

1. A two-component model, based on pure water and *ac9* measurements, was used. The pure water component was modeled with Pope and Fry's (1997) absorption values; *ac9* values were those measured at Site 2 on 1 June 1999 (Table 2). Scattering was modeled using the Petzold (1972) average particle phase function. Inelastic Raman scattering was also included in the calculations.
2. Downwelling solar irradiance (E_d) at the sea surface for the date of the overflight (1 June 1999) was calculated by a model in Hydrolight with atmospheric variables from a standard tropical area (sea level pressure = 758.69 mm Hg, humidity = 80%, water content = 2 cm).
3. The day 1 June 1999 was clear, so 0% cloud cover was used.

4. Wind speed was very low, but not calm. A wind speed of 2 m s^{-1} was used.
5. Reflectance spectra were selected from the three major environments (sediment, seagrass, and pavement/reef) and used to create a library representing 14 bottom types. All bottom types were assumed to be Lambertian and were created as follows.

Sediment: Oolitic sand (Sediment Type 1); oolitic-skeletal sand (Sediment Type 2) and sand with film (Sediment Type 3) were included. Sand in grass (Sediment Type 4), found only in combination with seagrass communities, was not represented as a unique bottom type.

Seagrass: The library includes spectra representing four densities of *Thalassia*: 20, 40, 60, and 80%. *Thalassia* reflectance was linearly mixed with that of Sediment Type 4 to make these community spectra. Density-dependent effects of the canopy structure, such as multiple scattering, were not modeled because a Lambertian bottom was assumed.

Pavement/Reef: The library includes spectra representing bare pavement, stony coral, and three typical hard-bottom pavement communities of light, medium, and dark color, as observed from video recordings. The community spectra were created by linearly mixing different percentages of gorgonians; (light and dark varieties) with sponges, fire coral *Millepora alcicornis*, the brown alga *Sargassum* sp., green alga *Microdictyon marinum*, and bare pavement. The mixture with the lowest reflectance, the “dark” pavement community, contained 45% gorgonians and sponges (35% light brown varieties, 10% dark brown varieties/sponges), 5% *Millepora alcicornis*, 5% *Sargassum* sp., 5% *Microdictyon*, and 40% bare pavement. The “medium” pavement community represented a mixture of 35% gorgonians and sponges (30% light brown, 5% dark brown/sponges), 5% *Millepora alcicornis*, 2.5% *Sargassum*, 2.5% *Microdictyon*, and 55% bare pavement. The “light” pavement community was a mixture of 23.3% gorgonians and sponges (20% light brown, 3.3% dark brown/sponges), 3.3% *Millepora alcicornis*, 3.3% *Sargassum*, and 70% bare pavement.

Spectral library verification—To verify the spectral library, simulated L_u spectra of Sediment Types 1 and 3 from 0.66 m below the surface were compared to in situ measurements of L_u made with the TSRB over these sediment types. Inputs to Hydrolight included IOP measurements, time and date of the TSRB run for calculation of sun angle, and depth from the TSRB sounder. IOP values represent ac_9 measurements taken at the time of TSRB runs. Results showed that Hydrolight simulations of L_u/E_d were generally within the range of TSRB L_u/E_d measurements (Fig. 5).

Image classification and error assessment

Hyperspectral PHILLS images were analyzed using the spectral library to create bottom type and bathymetric maps. Classification was performed using a minimum distance method in the software package ENVI 3.2 (Research Systems). Each pixel in the image was assigned the bottom type and depth corresponding to the spectrum in the library that

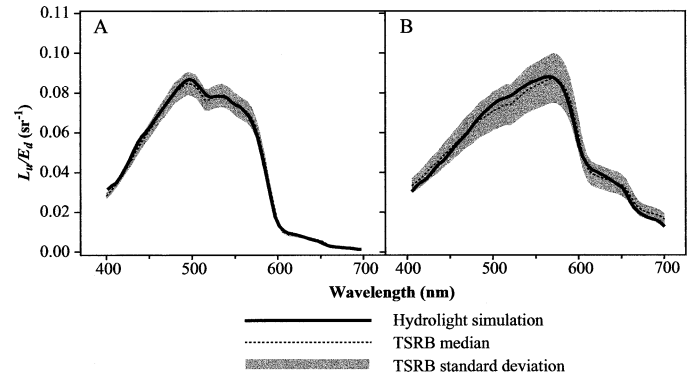


Fig. 5. Comparison of L_u/E_d from Hydrolight (L_u at a depth of 0.66 m) and TSRB measurements. Depth was measured using the TSRB sounder. (A) Oolitic sand (Sediment Type 1) at 5.0 m depth. (B) Peloidal-skeletal sand with algal film (Sediment Type 3) at 2.0 m depth.

most closely matched the PHILLS spectrum. A 5×5 -pixel median filter was used to remove stray pixels and reduce the resolution to below that of the multispectral IKONOS data used for georeferencing. Results were compared to ground truth maps of bottom type and bathymetric soundings to assess the accuracy of the spectral library approach, as outlined below.

Bottom type maps—Bottom classification maps generated for Sites 1 and 2 using the spectral library approach are shown in Fig. 6A,B. Comparisons between these maps and ground truth information based on the diver-generated bottom type map (Fig. 3) and observations from underwater video recordings and SCUBA dives indicate that, in general, the library bottom classification technique worked well. Specific points of comparison are as follows.

Site 1: Major features in the library classification map (Fig. 6A) and diver-generated ground truth map (Fig. 3) for Site 1 are similar. For example, a prominent shoal is evident in the middle of the maps, surrounded by beds of sparse seagrass. Pavement communities are also shown in both maps extending along the east and west sides.

Despite general similarities, some discrepancies between the two map types are apparent. Pavement communities are not as common in the library classification as in the ground truth map. This discrepancy is related, at least in part, to a difficulty in the library classification differentiating between dense seagrass (60–80%) and pavement bottom communities in water deeper than 8 m, where attenuation by water weakens the signal. In addition, the spectral library discriminated patches of ooid-skeletal sand (Sediment Type 2) within and at the edges of the ooid shoals, which were not distinguished in the ground truth map (Fig. 3). The influx of skeletal grains from adjacent seagrass beds and in the troughs of ooid sand waves was verified by field observations. This indicates the ability of spectral mapping to resolve fine-scale features.

Site 2: As in Site 1, bottom classification of Site 2 from the spectral library (Fig. 6B) shows a general correspondence with the ground truth map (Fig. 3). The dominant

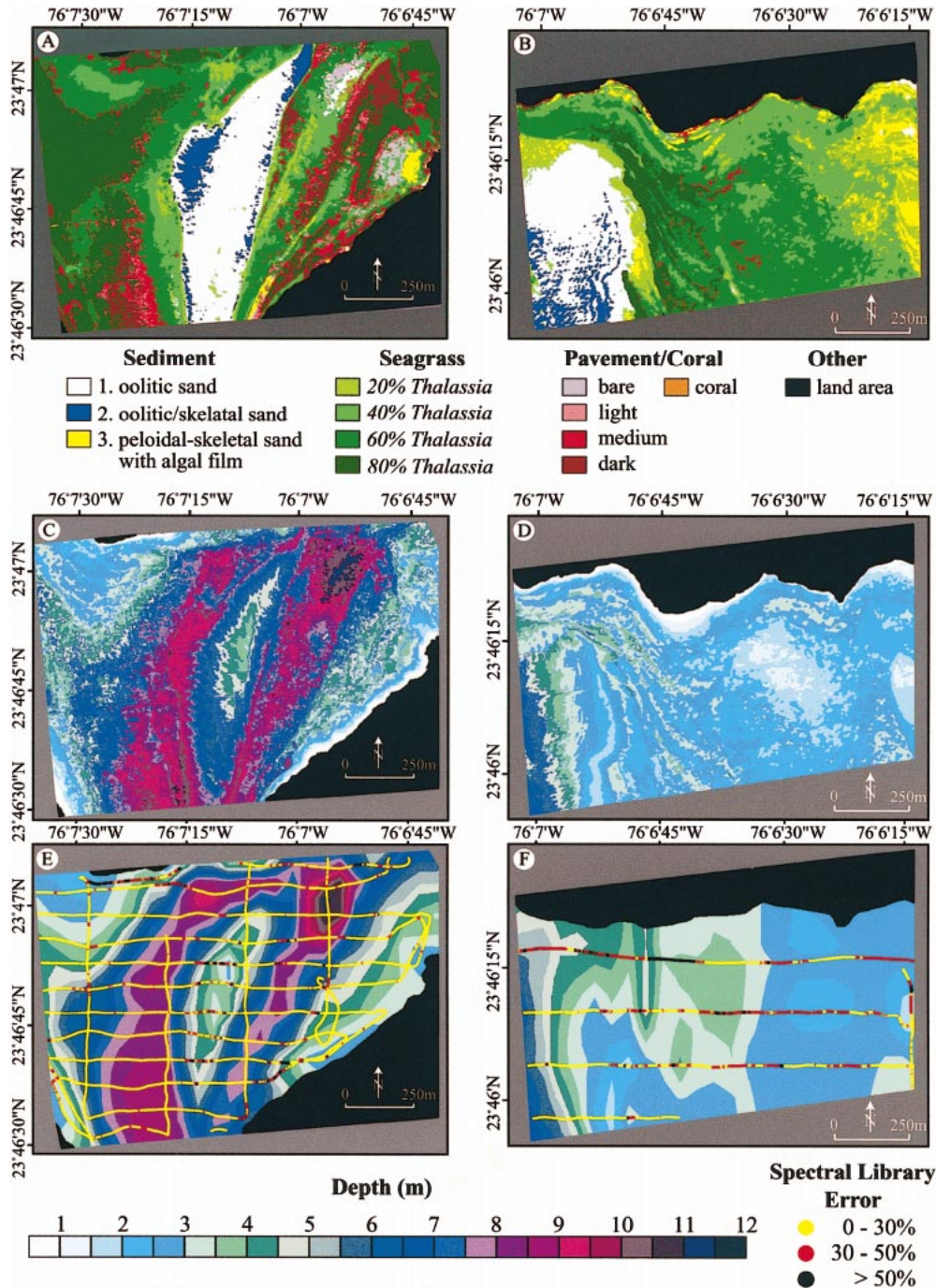


Fig. 6. Spectral library classification maps for bottom and bathymetry, with a comparison to ground truth bathymetry. (A) Spectral library bottom type, Site 1. (B) Spectral library bottom type, Site 2. (C) Spectral library bathymetry, Site 1. (D) Spectral library bathymetry, Site 2. (E) Ground truth bathymetry, Site 1. (F) Ground truth bathymetry, Site 2. Ground truth bathymetry maps were constructed by interpolating the sounder tracks shown in panels E and F. Depth at each point on the sounding track was compared to spectral library depth (panels C and D) to calculate error in spectral library classification. Apparent warping of the shoreline in the north of panels B and D is an artifact of the PHILLS camera.

features of Site 2 are a *Thalassia* meadow through the center, an ooid shoal on the western side, and film-coated sediment on the northeastern side.

Although most major features in both map types are in the correct positions, they do not match exactly in shape.

For example, the western shoal appears to be smaller in the ground truth map than the spectral library map. This was caused, at least in part, by the warping of the PHILLS image in the northwest corner, which made the island appear to bow inward and distort the shoal and seagrass. In addition,

there might have been a natural migration of the shoal in the time after the ground truth map was made in 1997, in part as a result of the effects of Hurricane Georges in 1998.

Additional field observations were conducted to investigate subtle differences between spectral library classification and ground truth maps as follows. (1) Spectral library maps show less extensive development of nearshore pavement than the ground truth map (island rim facies). Dives made in 1999 indicate, however, that nearshore pavement is commonly overlain with a few centimeters of sediment with sparse seagrass. These observations are consistent with spectral library classification of sparse seagrass in these nearshore areas. (2) Coral patch reefs in ground truth map were not classified in spectral library maps. Field observations indicate, however, that these reefs are small and that the coral is commonly overgrown by *Microdictyon marinum* and other algae. Observed coral heads with living polyps were smaller than the PHILLS pixel width of 1.25 m, making classification of coral unlikely. (3) Bioturbated seagrass beds on the eastern side of the ground truth map (Fig. 3) were classified by the spectral library as bioclastic peloidal-skeletal sand (Sediment Type 3) interspersed with sparse seagrass. Spectral library classification was confirmed by SCUBA dives, which showed this area to have large open patches of sediment with thick filmy layers and bioturbated mounds caused by burrowing shrimp. (4) Large fields of bioturbated sediment mounds near the shoreline in the northwest corner of Site 2 (Fig. 3) were mistakenly classified by the spectral library as patches of ooid sand (Sediment Type 1). Field observations indicate that these mounds consist of bright white sediment with little film. Additional work is needed to determine if these sediments can be spectrally distinguished from ooid sands.

Bathymetry maps—Bathymetry maps for Sites 1 and 2 derived using the spectral library approach are shown in Fig. 6C,D. These maps were compared to ground truth measurements of bathymetry made with the Suzuki echo sounder (Fig. 6D,E). Sounder depths were interpolated by a kriging method in the program “Surfer” (Golden Software). Percent error in spectral library bathymetry was calculated as follows.

$$\% \text{ error} = 100 \left(\frac{\text{depth}_{\text{spectral library}} - \text{depth}_{\text{sounder}}}{\text{depth}_{\text{sounder}}} \right) \quad (2)$$

The error in spectral library bathymetry was calculated only at points where depth sounder measurements were made (Fig. 6D,E).

Using combined data from both study sites, error calculations indicate that spectral library bathymetry has a mean accuracy of 83% (SD 13%, median accuracy 86%). Most of the error occurred in specific locations. Warping of the PHILLS image in Site 2 caused an error in georeferencing and an offset with ground truth soundings. The depth error was correspondingly high in the northern portion of Site 2, where the warping was greatest. Other errors in both Site 1 and Site 2 were found at the borders of the migrating shoal and at the island shoreline, where depth changed rapidly. Steeply sloped bottoms such as these were difficult to clas-

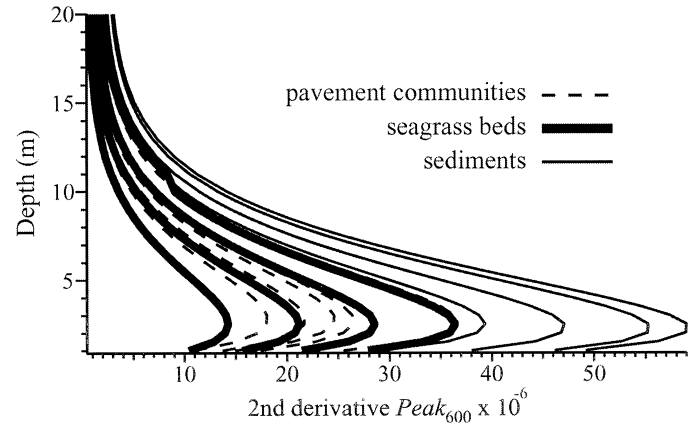


Fig. 7. Second derivative value at 600 nm for all bottom types in the spectral library.

sify at the time of the PHILLS overflight because the low sun angle created shadows on some portions of the slopes and increased reflectance on others. The spectral library was built under the assumption of a Lambertian bottom and would give spectral mismatches in these cases.

Spectroscopic analysis

Further analyses of library R_{rs} spectra were conducted in an attempt to find wavelengths that could be used in future models to estimate bathymetry or to classify sediment types. The large number of wavelength bands in hyperspectral data provided an opportunity to apply derivative spectroscopic techniques to finding these wavelengths. The second derivative, also known as the change in slope, at each wavelength of the modeled R_{rs} spectra was calculated using a 21-nm bandwidth (10 nm on either side of the wavelength point).

Analysis of the derivative data showed a major peak at 600 nm where the second derivative magnitude varied with water depth. This relationship was predictable, reflecting the change in the slope of reflectance from water attenuation, but it varied with different bottom types (Fig. 7). The variability with bottom types was minimized by dividing the peak height of the second derivative at 600 nm by the peak height of the second derivative at 515 nm, a region that varied less with depth and more with bottom type. Peak height at 600 nm was measured from the base at 627 nm. The base of the 515-nm peak was sloped, therefore the peak height at 515 nm was determined by using the function in Eq. 3.

$$\text{Peak}_{515} = \frac{d^2r}{d\lambda_{515 \text{ nm}}^2} - \left(\left[0.5 \cdot \frac{d^2r}{d\lambda_{547 \text{ nm}}^2} \right] + 3.0 \times 10^{-7} \right) \quad (3)$$

The ratio $\text{Peak}_{600}/\text{Peak}_{515}$ was plotted versus depth to show that bathymetry can be estimated based solely on the derivative spectra of reflectance (Fig. 8). Two distinct bathymetric relationships emerged: one for sediment and seagrass and the other for pavement bottoms with soft corals. These relationships could be used together to determine bathymetry, if bottom types were classified beforehand into either sediment/seagrass or pavement communities, possibly by using

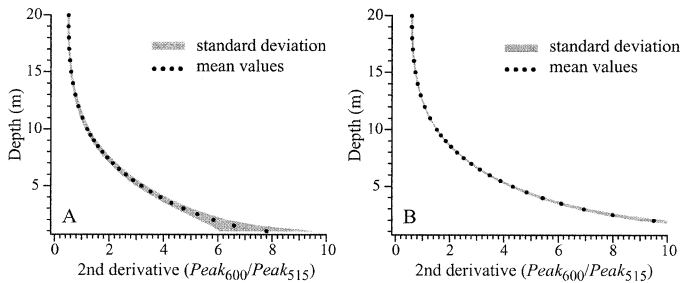


Fig. 8. Mean of second derivative peak ratio ($\text{Peak}_{600}/\text{Peak}_{515}$) versus depth for spectral library. (A) Sediment and seagrass. (B) Pavement/reef.

another spectral indicator. Additional research into the physical and biological factors of spectral reflectance will be needed to define derivative relationships with bottom types. Initial results, however, indicate that hyperspectral data contain valuable information that can be used for future remote sensing studies of benthic habitats.

Our study indicates that a spectral library approach was effective in mapping benthic environments and estimating bathymetry in the clear waters surrounding Lee Stocking Island. The principal methods and results are summarized as follows.

1. A library of remote sensing reflectance (R_{rs}) spectra was built from the simulated R_{rs} output of Hydrolight. Inputs included bottom reflectance spectra from sediments, seagrass, and pavement communities; measured water inherent optical properties; and environmental variables from Lee Stocking Island, Bahamas. Simulated R_{rs} spectra were created for water depths ranging from 1 to 10 m at 0.5-m increments and from 10 to 20 m at 1-m increments.
2. Hydrolight output was verified by comparing simulated L_u/E_d spectra to L_u/E_d measured with a spectral radiometer buoy over sediment end members. There was a close match in spectral shape and magnitude between calculated and measured spectra.
3. The spectral library was used to classify a hyperspectral image taken with a PHILLS airborne sensor at LSI on 1 June 1999 at 1400–1500 h GMT. The image was classified by bottom type and bathymetry using a minimum distance method in ENVI 3.2. The resulting bottom type map corresponded well to an existing ground truth map and displayed details that were verified by direct diver observation. Spectral library bathymetry had a mean accuracy of 83% and median accuracy of 86% compared to measured depth soundings.
4. Spectroscopic analysis of simulated R_{rs} spectra showed that the ratio of the second derivative at 600 nm to that at 515 nm can be used to determine water depth.

The progression from multispectral to hyperspectral imaging is a technological leap that provides the capability to distinguish between closely related bottom types. Even carbonate sediments with similar reflectance spectra were found to have sufficient spectral variation to enable benthic classification. The results of library classification indicate that these spectral differences can be exploited using simple matching routines and can be used for bathymetric estima-

tions. The creation of more and larger spectral libraries will extend the regional use of this type of mapping and will aid in constructing better optical models to analyze hyperspectral data.

Derivative algorithms show great promise in identifying important spectral regions and quantifying parameters such as water depth and sediment chlorophyll content. With improvements in satellite sensor technology, such as increased signal to noise ratios and higher pixel resolution, derivative algorithms and other spectroscopic analysis techniques will become a valuable tool in deciphering complex benthic optical signatures.

References

- BROTAS, V., T. CABRITA, A. PORTUGAL, J. SERODIO, AND F. CATARINO. 1995. Spatio-temporal distribution of the microphytobenthic biomass in intertidal flats of Targus Estuary (Portugal). *Hydrobiologia* **300/301**: 93–104.
- BUTLER, W. L. AND D. W. HOPKINS. 1970. Higher derivative analysis of complex absorption spectra. *Photochem. Photobiol.* **12**: 439–450.
- CLARK, R. N., G. A. SWAYZE, AND A. GALLAGHER. 1992. Mapping the mineralogy and lithology of Canyonlands, Utah with imaging spectrometer data and the multiple spectral feature mapping algorithm. Summaries of the Third Annual JPL Airborne Geosciences Workshop. V. 1: AVIRIS Workshop. JPL Publ. **92**: 11–13.
- , ———, ———, T. V. V. KING, AND W. M. CALVIN. 1993. The U.S. Geological Survey, Digital Spectral Library: Version 1: 0.2 to 3.0 μm . U.S. Geological Survey Open File Report 93-592.
- , T. V. V. KING, C. AGER, AND G. A. SWAYZE. 1995. Initial vegetation species and senescence/stress mapping in the San Luis Valley, Colorado using imaging spectrometer data, p. 64. *In* H. H. Posey, J. A. Pendleton, and D. Van Zyl [eds.], *Proceedings: Summitville Forum '95*. V. 38. Colorado Geological Survey Special Publication.
- CURRAN, P. J., J. L. DUNGAN, B. A. MACLER, S. E. PLUMMER, AND D. L. PETERSON. 1992. Reflectance spectroscopy of fresh whole leaves for the estimation of chemical concentration. *Remote Sens. Environ.* **39**: 153–166.
- DAVIS, C. O., AND OTHERS. 2002. Ocean PHILLS hyperspectral imager: Design, characterization, and calibration. *Opt. Express* **10**: 210–221.
- , M. KAPPUS, J. BOWLES, J. FISHER, J. ANTONIADES, AND M. CARNEY. 1999. Calibration, characterization, and first results with the Ocean PHILLS hyperspectral imager. *Proc. SPIE Conf. Imag. Spectrom.* **3753**: 160–168.
- DEMETRIADES-SHAH, T. H., M. D. STEVEN, AND J. A. CLARK. 1990. High resolution derivative spectra in remote sensing. *Remote Sens. Environ.* **33**: 55–64.
- GAO, B., M. J. MONTES, Z. AHMAD, AND C. O. DAVIS. 2000. Atmospheric correction algorithm for hyperspectral remote sensing of ocean color from space. *Appl. Opt.* **39**: 887–896.
- GONZALEZ, R., AND G. P. EBERLI. 1997. Sediment transport and sedimentary structures in a carbonate tidal inlet; Lee Stocking Island, Exuma Islands, Bahamas. *Sedimentology* **44**: 1015–1030.
- HARRIS, P. M., AND W. S. KOWALIK. 1994. Satellite images of carbonate depositional settings. *American Association of Petroleum Geologists Methods in Exploration Ser. 11*.
- HIROI, T., AND C. M. PIETERS. 1992. Effects of grain size and shape

- in modeling reflectance spectra of mineral mixtures. *Proc. Lunar Planet. Sci.* **22**: 313–325.
- , AND ———. 1994. Estimation of grain sizes and mixing ratios of fine powder mixtures of common geologic minerals. *J. Geophys. Res.* **99**: 10,867–10,879.
- HOLDEN, H., AND E. LEDREW. 1998. Monitoring the health of coral reefs. *Backscatter: Aquat. Inf. Technol.* **9**(3): 28–31.
- HU, C., F. MULLER-KARGER, K. L. CARDER, AND Z. LEE. 1998. A method to derive optical properties over shallow waters using Seawifs. *In* S. G. Ackleson [ed.], *Proc. Ocean Optics XV (CD-ROM)*. Paper no. 1138, 6.
- HUGUENIN, R. L., AND J. L. JONES. 1986. Intelligent information extraction from reflectance spectra: Absorption band position. *J. Geophys. Res.* **91**(B9): 9585–9598.
- JERLOV, N. G. 1976. *Marine optics*. Elsevier.
- KARNIELI, A., J. G. KIDRON, C. GLAESSER, AND E. BEN-DOR. 1999. Spectral characteristics of cyanobacterial soil crust in semiarid environments. *Remote Sens. Environ.* **69**: 67–75.
- KIRK, T. O. 1994. *Light and photosynthesis in aquatic ecosystems*, 2nd ed. Cambridge Univ. Press.
- KOKALY, R. F., AND R. N. CLARK. 1999. Spectroscopic determination of leaf biochemistry using band-depth analysis of absorption features and stepwise multiple linear regression. *Remote Sens. Environ.* **67**: 267–287.
- LEE, Z., K. L. CARDER, R. G. STEWARD, T. G. PEACOCK, C. O. DAVIS, AND J. L. MUELLER. 1997. Remote sensing reflectance and inherent optical properties of oceanic waters derived from above-water measurements. *In* S. G. Ackleson [ed.], *Ocean optics XIII. Proc. SPIE* **2963**: 160–166.
- LYZENGA, D. R. 1981. Remote sensing of bottom reflectance and water attenuation parameter in shallow water using aircraft and Landsat data. *Int. J. Remote Sens.* **2**: 71.
- MARITORENA, S., A. MOREL, AND B. GENTILI. 1994. Diffuse reflectance of oceanic shallow waters: Influence of water depth and bottom albedo. *Limnol. Oceanogr.* **39**: 1689–1703.
- MAZEL, C. H. 1997. Diver-operated instrument for in situ measurement of spectral fluorescence and reflectance in benthic marine organisms and substrates. *Opt. Eng.* **36**: 2612–2617.
- MILLIMAN, J. D. 1974. *Recent sedimentary carbonates part 1: Marine carbonates*. Springer-Verlag.
- PALACIOS-ORUETA, A., AND S. L. USTIN. 1998. Remote sensing of soil properties in the Santa Monica Mountains I. Spectral analysis. *Remote Sens. Environ.* **65**: 170–183.
- PATTERSON, D. M., AND OTHERS. 1998. Microbiological mediation of spectral reflectance from intertidal cohesive sediments. *Limnol. Oceanogr.* **43**: 1207–1221.
- PETZOLD, T. J. 1972. Volume scattering function for selected ocean waters. *SIO Ref. 72–78*; Scripps Institute of Oceanography.
- PHILPOT, W. D. 1988. Bathymetric mapping with passive multispectral imagery. *Appl. Opt.* **28**: 1569–1578.
- . 1990. The derivative ratio algorithm: Avoiding atmospheric effects in remote sensing. *IEEE Trans. Geosci. Remote Sens.* **29**: 350–357.
- POPE, R. M., AND E. S. FRY. 1997. Absorption spectrum (380–700 nm) of pure water. II. Integrating cavity measurements. *Appl. Opt.* **36**: 8710–8723.
- ROLLIN, E. M., AND E. J. MILTON. 1998. Processing of high spectral resolution reflectance data for the retrieval of canopy water content information. *Remote Sens. Environ.* **65**: 86–92.
- STEPHENS, F. C., E. M. LOUCHARD, R. P. REID, R. A. MAFFIONE. 2003. Effects of microalgal communities on reflectance spectra of carbonate sediments in subtidal optically shallow marine environments. *Limnol. Oceanogr.* **48**: 535–546.
- TWARDOWSKI, M. S., J. M. SULLIVAN, P. L. DONAGHAY, J. R. V. ZANEVELD. 1999. Microscale quantification of the absorption by dissolved and particulate material in coastal waters with an *ac9*. *J. Atm. Ocean. Tech.* **16**: 691–707.
- ZIMMERMAN, R.C. AND S.K. WITTLINGER. 2000. Hyperspectral remote sensing of submerged aquatic vegetation in optically shallow waters. *Ocean Optics XV, Monaco*.

Received: 1 October 2001

Accepted: 30 April 2002

Amended: 4 July 2002